Optics Letters

Design rules for combined label-free and fluorescence Bloch surface wave biosensors

Francesco Michelotti,[1,*] Riccardo Rizzo,[1,2] Alberto Sinibaldi,[1] Peter Munzert,[2] Christoph Wächter,[2] and Norbert Danz[2]

[1]Dipartimento di Scienze di Base e Applicate per l'Ingegneria, SAPIENZA Università di Roma, Via A. Scarpa 16, 00161 Rome, Italy
[2]Fraunhofer Institute for Applied Optics and Engineering, Albert Einstein Strasse 7, 07745 Jena, Germany
*Corresponding author: francesco.michelotti@uniroma1.it

Received 10 May 2017; revised 16 June 2017; accepted 19 June 2017; posted 21 June 2017 (Doc. ID 295409); published 11 July 2017

We report on the fabrication and physical characterization of optical biosensors implementing simultaneous label-free and fluorescence detection and taking advantage of the excitation of Bloch surface waves at a photonic crystal's truncation interface. Two types of purposely designed one-dimensional photonic crystals on molded organic substrates with micro-optics were fabricated. These crystals feature either high or low finesse of the Bloch surface wave resonances and were tested on the same optical readout system. The experimental results show that designing biochips with a large resonance quality factor does not necessarily lead in the real case to an improvement of the biosensor performance. The conditions for optimal biochip design and operation of the complete bio-sensing platform are established.

OCIS codes: (280.4788) Optical sensing and sensors; (280.1415) Biological sensing and sensors; (240.6690) Surface waves; (230.5298) Photonic crystals.

https://doi.org/10.1364/OL.42.002798

Optical sensors based on the resonant excitation of electromagnetic surface waves are widely diffused in the field of biochemical binding analysis. In particular, surface plasmon resonance (SPR) is involved in many label-free (LF) sensing platforms due to the sensitivity, resolution, and simplicity of the detection scheme [1]. Recently, Bloch surface waves (BSWs) [2] sustained at the interface between a finite one-dimensional photonic crystal (1D-PC) and an external medium were proposed as an alternative to SPR [3,4]. They feature an improved limit of detection [5] and the possibility to operate in a wide spectral range from the visible to the terahertz region, when properly selecting the 1D-PC materials and geometry [6,7]. Coupling to BSW has also been demonstrated to improve the excitation and collection of the fluorescence (FLUO) emitted by molecules at the surface of a low-loss dielectric 1D-PC [8].

Recently, we reported on the development of sensing platforms implementing simultaneous LF and FLUO detection, based on BSW and operating in either the near infrared [9] or visible [10] ranges. Such an approach aims at increasing the resolution by simultaneously collecting complementary signals, similar to other configurations [11,12].

In this Letter, we report on the design, fabrication, and experimental characterization of BSW sensors featuring two different 1D-PC designs. The aim is to identify the route to optimized sensors integrating both LF and FLUO operation in the visible range [10], respectively, at $\lambda_{\mathrm{LF}} = 670$ nm and $\lambda_{\mathrm{FLUO}} \in [670\ \mathrm{nm}, 750\ \mathrm{nm}]$ for photo-excitation carried out at $\lambda_{\mathrm{EXC}} = 635$ nm.

The 1D-PC used in the experiments are dielectric multilayers deposited on cyclic olefin copolymer (TOPAS) substrates [13,14] by plasma-ion-assisted deposition under high vacuum [15].

The geometries of the two sensor types (Table 1) share a common periodic multilayer and are terminated by two different thin dielectric bi-layers. SiO_2 and Ta_2O_5 are the low- and high-index dielectric materials used to fabricate the periodic part, with N periods; the complex refractive indices are $n_L = 1.474 + i5 * 10^{-6}$ and $n_H = 2.106 + i5 * 10^{-5}$ at λ_{LF}, respectively. The thin dielectric bi-layer is either Ta_2O_5/SiO_2 or TiO_2/SiO_2, for Type 1 and 2 sensors, respectively. TiO_2 has a complex refractive index $n'_H = 2.28 + i1.8 * 10^{-3}$ at λ_{LF}. In the topping bi-layer, the role of the first high-index layer (Ta_2O_5 or TiO_2) is to tailor the BSW properties to improve the LF biosensing performance, while the second layer (SiO_2) provides a surface that can be treated with standardized and reliable silane-based chemical functionalization protocols [10].

The TOPAS substrates ($n_{\mathrm{TOPAS}} = 1.530$ at λ_{LF}) were fabricated by injection molding and include two cylindrically shaped input and output optical windows, as shown in Fig. 1. The substrates fit to the optical reading system of an integrated platform designed and fabricated to operate in both LF and FLUO modes. The illumination is focused cylindrically along the incidence plane to a line at the surface of the chip. The output cylindrical window of the chip (output diopter) is used to collect the reflected/emitted light and performs optical Fourier transformation at the CCD (Sony ICX205AL) array sensor along the incidence plane direction.

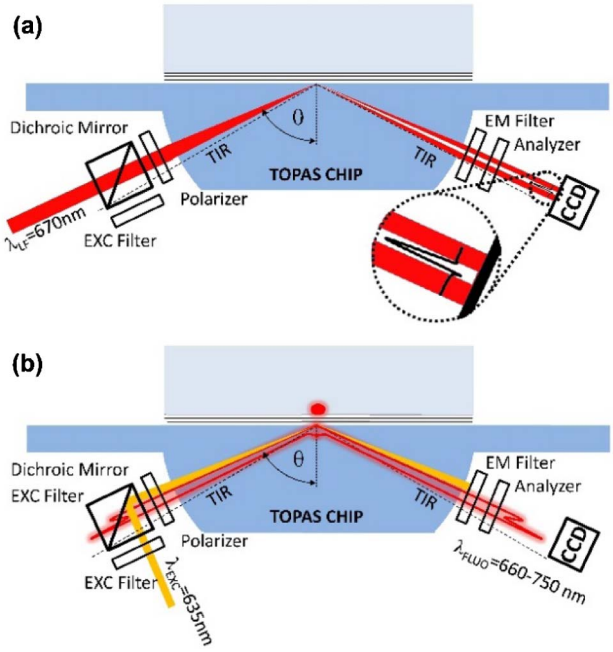

Fig. 1. Sketch of the optical configuration of the sensing platform for the (a) LF operation and the (b) FLUO operation. For the sake of clarity, in the sketch we did not draw the beam shaping optics and beam steering mechanics. Dimensions are not to scale.

As shown in Fig. 1(a), in the LF mode, a collimated laser beam at λ_{LF} is focused at the chip surface above the total internal reflection (TIR) angle, and the reflected beam is collected by the CCD array in a 4 deg angular window. Destruction of the spatial coherence by means of a rotating diffuser (not shown), combined with the CCD integration time, avoids image degradation due to speckles. In such a Kretschmann–Raether configuration [16], the excitation of a BSW gives rise to a dip in the angular reflectance spectrum that is transformed by the output diopter to a dip in the intensity distribution along the CCD long axis (1280 pixel, in the incidence plane).

In the FLUO mode [see Fig. 1(b)], we use a BSW for both FLUO excitation and collection. A collimated laser beam at λ_{EXC} is focused in a narrower angular range ($\Delta\theta_{\mathrm{EXC}} \sim 2$ deg). A combination of a dichroic mirror and excitation and emission filters (Chroma, F46-112 633-640 nm ET Laser Filter Set) limits stray light effects. Parallel steering in the incidence plane of the FLUO excitation beam (not shown in Fig. 1) allows one to tune the incidence angle θ_{EXC} to match the BSW angle θ_{BSW} at λ_{EXC}, and excite fluorophores placed at the chip surface via a resonant BSW mode. Previous works [8] demonstrated that the field localization due to the excitation of a BSW gives rise to a strong increase of the excitation rate. Moreover, the broad emission spectrum of the fluorophores is coupled to polychromatic BSWs, which leak into the substrate in a narrow angular range [17], and are collected by the same CCD. The output diopter, combined with the dispersion of the BSW, images every spectral component of the emission with a one-to-one mapping onto a different position of the CCD [9,10].

In both the LF and the FLUO operation, the intensity along the CCD short axis (1024 pixel) corresponds to different positions along the illuminated strip at the chip surface, allowing sensing of several spots at the same time [14]. A polarizer can set the linear polarization of the incident light and an analyzer, as shown in Fig. 1, analyzes that of the reflected/emitted light.

Table 1. Geometry of Type 1 and 2 Sensors

			Periodic 1D-PC		Topping Bi-Layer	
Type	Geometry	N	d_H [nm]	d_L	d'_H [nm]	d'_L
1	$L(\mathrm{HL})^N H'L'$	3	120	340	Ta_2O_5 20	SiO_2 20
2		2	120	275	TiO_2 20	SiO_2 20

The 1D-PC geometries resumed in Table 1 were designed to show either a narrow or a broad BSW dip in the LF angular reflectance spectrum R_{TE} for the TE polarization. In Figs. 2(a) and 3(a), we show the theoretical R_{TE} at λ_{LF} for the two sensor types, calculated [16] assuming a TOPAS substrate ($n_{\mathrm{TOPAS}} = 1.530$) and water as an external medium ($n_{\mathrm{EXT}} = 1.330$). For both types, deep resonances at θ_{BSW} are expected for the TE-polarized BSW, which are strongly localized at the 1D-PC sensor surface. The sensors also feature shallow and broad TM resonances, corresponding to modes that are more extended inside the 1D-PC structure.

In Table 2, we list the values of the full width at half-maximum (W) and resonance depth (D) for all dips appearing in Figs. 2(a) and 3(a), together with their calculated volume sensitivity $S_{\mathrm{LF}} = d\theta_{\mathrm{BSW}}/dn_{\mathrm{EXT}}$. From the values found for W, D, and S_{LF}, one can evaluate the figure of merit for the LF performance defined as $\mathrm{FoM}_{\mathrm{LF}} = S * D/W$ [16], which is also listed in Table 2. We also list the calculated field

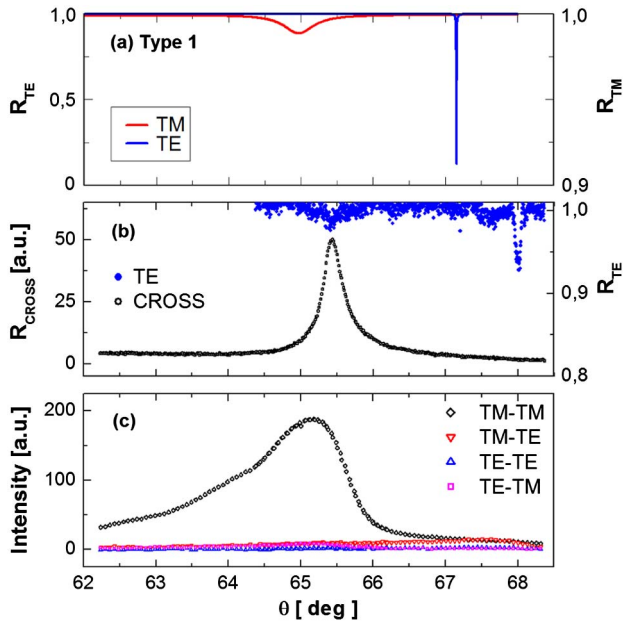

Fig. 2. Type 1. (a) Simulated angular TIR reflectance, (b) experimental reflectance in the TE and CROSS configuration, and (c) FLUO emission for four different excitation (first label) and collection (second label) polarizations.

enhancement factor (FEF), defined as the ratio of the amplitude of the field at the sensor/water interface to that of the field in TOPAS, when the chips are excited at λ_{EXC} at the TE θ_{BSW}.

Among all cases, the Type 1 sensor displays the best design FoM_{LF} and FEF (TE pol), which could suggest it as a first choice for both LF and FLUO biosensing applications. However, as it will be clear from the experimental results reported below, the best choice reveals to be that of a Type 2 sensor instead.

In Figs. 2(b) and 3(b), we show the angular LF reflectance measured experimentally when operating the chips on the platform of Fig. 1, for Type 1 and 2, respectively. Data were obtained by averaging 30 CCD lines, corresponding to a 260 μm wide spot on the chip surface (also for FLUO operation).

In the TE case (red), sharp resonant dips are found. As expected, the resonant TM dips are hardly observed (not shown); however, their angular position can be probed by operating the platform in a phase-sensitive configuration (CROSS), where the two polarizers are turned by 45 deg with respect to the incidence plane. Under such conditions, the overall reflectance R_{CROSS} is sensitive to the amplitude and phase of the TE and TM reflected components [16]. In Figs. 2(b) and 3(b), the experimental R_{CROSS} (black) shows resonances around the expected position of the TM modes and permits us to identify them.

Besides allowing for mode spectroscopy and characterization, working in the CROSS configuration is very desirable for sensing applications, as it permits increasing the FoM when the 1D-PCs are characterized by extremely small losses (and small D) [16]. For this reason, polarizers were implemented in the integrated optical platform. We point out that in the CROSS case the S_{LF} coincides with that of either the TE or the TM single polarization case, depending on the resonance that is exploited [16].

For both sensor types, the BSW resonances are slightly shifted with respect to the theoretical position. For Type 1, the TE dip is much wider and shallower than the theoretical prediction while, for Type 2, the dip, which is wider by design, is not much broadened and keeps relatively deep. Such effects are ascribed, for both Type 1 and 2, to the 1D-PC layers' thickness fabrication tolerances [18] and to the plastic substrate optical quality [5]. Additionally, for Type 2, the TiO_2 absorption loss might differ from that assumed for the simulations.

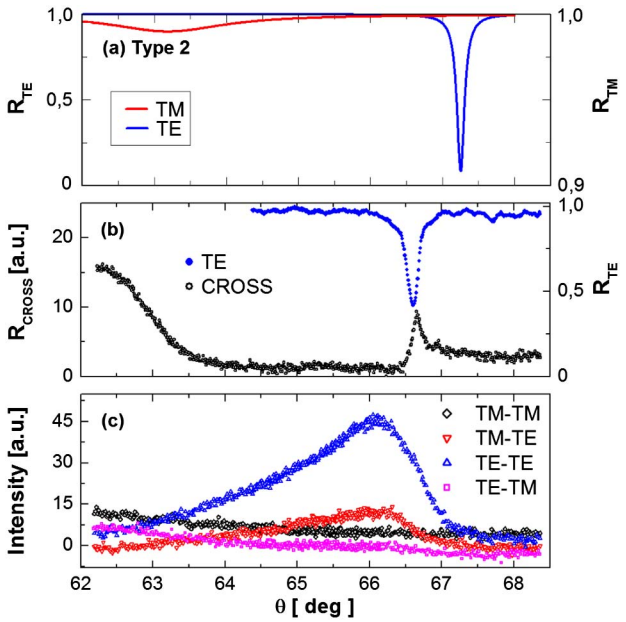

Fig. 3. Type 2. (a) Simulated angular TIR reflectance, (b) experimental reflectance in the TE and CROSS configuration, and (c) FLUO emission for four different excitation (first label) and collection (second label) polarizations.

Reference measurements carried out with the same 1D-PC deposited on microscope slides show that the higher optical quality of the substrates preserves the dips' W (not reported here).

From the LF measurements, we extracted the experimental values for W, D, and S_{LF} shown in Table 2. The S_{LF} values were measured experimentally by using different known solutions of glucose in doubly deionized water [5]; in the TM BSW case (Type 1 only), S_{LF} was measured in the CROSS configuration. In Table 2, the experimental values for the FoM are significantly reduced compared to theoretical predictions and indicate that the Type 2 sensor shows the best LF performance. For comparison, we report also the FoM_{LF} for a SPR sensor operating at $\lambda_{LF} = 804$ nm [5] showing that, indeed, the present 1D-PC provides improved LF performance.

Figures 2(b) and 3(b) also show that the CROSS operation enhances the TE and TM response of Type 2 sensors whereas, for Type 1, the TM resonance is enhanced, but the TE is depressed. The last result is due to a reduced phase shift ($<2\pi$) of the TE reflection coefficient across such a high finesse resonance [16].

In Figs. 2(c) and 3(c), we show measurements carried out in the FLUO mode in a water environment. Before carrying on the measurements, the surface of the sensors was stained with a 10 nM solution of Nile Blue (NB) dye (Radiant Dyes, $\lambda_{MAX} = 685$ nm) [19] in deionized water and rinsed repetitively. The gain and integration time of the CCD were increased with respect to the LF case.

The FLUO emission curves were obtained by exciting at λ_{EXC} with either TE or TM polarization and detecting FLUO along either the TE or the TM polarization. Depending on the polarization, the excitation angle θ_{EXC} was tuned to the respective resonance by maximizing the FLUO signal, if present. As the NB molecules are free to rotate, their orientation is lost due to rotational randomization in the NB excited state [20]; therefore, NB molecules can be assumed to be isotropically oriented and couple to both TE- and TM-polarized BSWs of the 1D-PC.

For Type 1 [Fig. 2(c)], relatively intense FLUO was measured only for the TM–TM case. Owing to the dispersion of the TM BSW mode, each spectral component of the emission at $\lambda > \lambda_{EXC}$ is coupled out at a different angle $\theta < \theta_{EXC}$. Given that for NB $\lambda_{MAX} > \lambda_{LF} > \lambda_{EXC}$, the angular FLUO distribution lies on the small angle side of the resonance observed in the LF mode at λ_{LF}. The NB FLUO coupled to the TM BSW is channeled in a 4 deg angular window and can be efficiently detected by the same optical system used for LF operation. Only a faint TM–TE FLUO signal is observed on the small angle side of the TE resonance in the LF mode, despite the extremely large theoretical FEF of the TE mode. TE excitation does not give rise to any appreciable FLUO signal.

For Type 2 [Fig. 3(c)], relatively intense FLUO was measured for all TM–TE combinations, with angular distribution that lies on the small angles side of the respective LF resonance. The TM FLUO, however, peaks outside the observation

Table 2. Theoretical and Experimental Values of the Relevant Parameters for the Two 1D-PC Designs

		Theory					Experiment			
				λ_{LF}		λ_{EXC}			λ_{LF}	
Type	Pol	W [mdeg]	D	S_{LF} [deg/RIU]	FoM_{LF}[RIU^{-1}]	FEF	W [mdeg]	D	S_{LF} [deg/RIU]	FoM_{LF}[RIU^{-1}]
1	TE	6	0.85	29.4	4165	64	60	0.08	26.7	35.6
	TM	550	0.01	22.7	0.41	8	NA	NA	21.3	NA
2	TE	140	0.90	35.4	227	16	200	0.55	31.8	87.5
	TM	2090	0.01	33.7	0.16	4	NA	NA	NA	NA
SPR	TM	After Ref. [5], $\lambda_{LF} = 804$ nm					1470	0.76	80.1	41.4

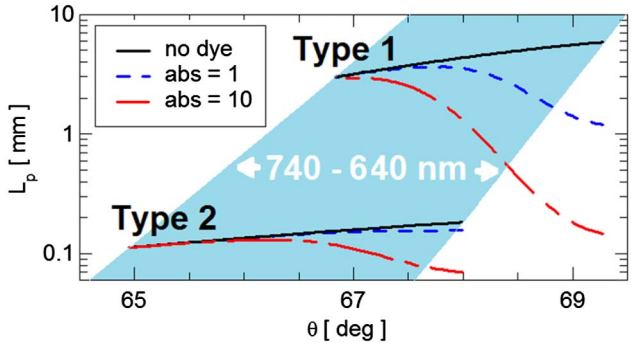

Fig. 4. Calculated L_p for both Type 1 and 2 design sensors. No dye and no absorption losses (solid), arbitrary 1-fold (dashed) and 10-fold (dot-dashed) NB dye absorption at the 1D-PC surface. The light blue region is just a guide for the eye, suggesting that the same spectral emission range for the NB dye corresponds to different angular ranges for the two types, due to the different BSW dispersion.

window at smaller angles. As expected from the FEF values, the TE-emitted FLUO is larger for TE than for TM excitation. The intensities found in Figs. 3(c) and 2(c), however, cannot be compared, because the NB staining procedure suffers from poor reproducibility and does not permit us to control the NB surface density.

The completely different FLUO characteristics observed for the two types of sensors can be ascribed to the following causes.

First, the NB dye excitation rate depends on the FEF of the BSW at λ_{EXC} and on the ratio $\eta = W/\Delta\theta_{EXC}$. For the Type 1 sensor, $\eta \sim 3\%$ for the TE polarization and, despite the largest FEF, the excitation rate is small. On the other hand, for Type 1 (TM pol) and Type 2, η is larger and, consequently, the excitation rate is improved.

Secondly, the propagation length L_p of the TE BSW mode, excited by spontaneous emission, before radiating in the substrate is extremely large in Type 1 sensors. In Fig. 4, we show the calculation of L_p in the TE case, carried out with a commercial mode solver for the two sensor types (the TM values are more than 10 times smaller). We performed the calculations for several different arbitrary values of the NB dye absorption. As the effect of increasing NB dye absorption losses at the 1D-PC surface shown in Fig. 4 illustrates, the increased L_p also sensitizes the stack for reabsorption. As a consequence, for Type 1 (TE pol), L_p is so large that the emitted energy is strongly reabsorbed by the NB dye, and the remaining energy leaves the 1D-PC outside the spatial field of view of the detection optics, which is about 2 mm.

In conclusion, we can state that designing 1D-PC with extremely sharp resonances does not necessarily lead to improved LF and FLUO sensors. For LF sensing, the design must carefully take into account the fabrication tolerances and the substrate quality that limit the FoM_{LF}. For FLUO applications, the sharpness of a resonance converts into a large propagation length, which governs both the angular matching of the excitation beam to the incoupling BSW and the extraction of the outcoupling BSW in terms of real-space widths of the collecting system. This must be kept in mind also for applications in FLUO microscopy. The Type 2 design allows for a FoM_{LF} which outperforms SPR and, at the same time, permits us to operate efficiently in a FLUO mode.

Funding. Seventh Framework Programme (FP7) BILOBA (318035).

REFERENCES

1. M. Piliarik and J. Homola, Opt. Express **17**, 16505 (2009).
2. P. Yeh, A. Yariv, and C.-S. Hong, J. Opt. Soc. Am. **67**, 423 (1977).
3. M. Shinn and W. M. Robertson, Sens. Actuators B **105**, 360 (2005).
4. V. N. Konopsky and E. V. Alieva, Anal. Chem. **79**, 4729 (2007).
5. A. Sinibaldi, N. Danz, E. Descrovi, P. Munzert, U. Schulz, F. Sonntag, L. Dominici, and F. Michelotti, Sens. Actuators B **174**, 292 (2012).
6. A. Farmer, A. Friedli, S. M. Wright, and W. M. Robertson, Sens. Actuators B **173**, 79 (2012).
7. V. Paeder, J. Darmo, and K. Unterrainer, *IEEE 38th International Conference on Infrared, Millimeter, and Terahertz Waves (IRMMW-THz)* (2013).
8. J. Y. Ye and M. Ishikawa, Opt. Lett. **33**, 1729 (2008).
9. A. Sinibaldi, A. Fieramosca, R. Rizzo, A. Anopchenko, N. Danz, P. Munzert, C. Magistris, C. Barolo, and F. Michelotti, Opt. Lett. **39**, 2947 (2014).
10. A. Sinibaldi, C. Sampaoli, N. Danz, P. Munzert, L. Sibilio, F. Sonntag, A. Occhicone, E. Falvo, E. Tremante, P. Giacomini, and F. Michelotti, Biosens. Bioelectron. **92**, 125 (2017).
11. C. Mathias, N. Ganesh, L. L. Chan, and B. T. Cunningham, Appl. Opt. **46**, 2351 (2007).
12. K. Toma, M. Vala, P. Adam, J. Homola, W. Knoll, and J. Dostálek, Opt. Express **21**, 10121 (2013).
13. http://www.topas.com/sites/default/files/files/TOPAS_Brochure_E_2014_06%281%29.pdf.
14. N. Danz, A. Kick, F. Sonntag, S. Schmieder, B. Höfer, U. Klotzbach, and M. Mertig, Eng. Life Sci. **11**, 566 (2011).
15. P. Munzert, N. Danz, A. Sinibaldi, and F. Michelotti, Surf. Coat. Technol. **314**, 79 (2017).
16. A. Sinibaldi, R. Rizzo, G. Figliozzi, E. Descrovi, N. Danz, P. Munzert, A. Anopchenko, and F. Michelotti, Opt. Express **21**, 23331 (2013).
17. R. Badugu, K. Nowazcyk, E. Descrovi, and J. R. Lakowicz, Anal. Biochem. **442**, 83 (2013).
18. R. C. Nesnidal and T. G. Walker, Appl. Opt. **35**, 2226 (1996).
19. http://www.radiant-dyes.com/index.php, Nilblau perchlorate (Cat.N.98).
20. F. Perrin, J. Phys. **7**, 390 (1926).